Modeling by Assembly and Molecular Dynamics Simulations of the Low Cu^{2+} Occupancy Form of the Mammalian Prion Protein Octarepeat Region: Gaining Insight into Cu^{2+}-Mediated β-Cleavage

M. Jake Pushie and Hans J. Vogel
Structural Biology Research Group, Department of Biological Sciences, University of Calgary, Calgary, Alberta T2N 1N4, Canada

ABSTRACT The prion protein has garnered considerable interest because of its involvement in prion disease as well as its unresolved cellular function. The octarepeat region in the flexible N-domain is capable of binding copper through multiple coordination modes. Under conditions of low pH and low Cu^{2+} concentration, the four octarepeats (ORs) cooperatively coordinate a single copper ion. Based on the average structure of the PHGG and GWGQ portions of a copper-free OR_2 model from molecular dynamics simulations, the starting structures of the OR_4 complex could be constructed by assembling the repeating structure of PHGG and GWGQ fragments. The resulting model contains a preformed site suitable for Cu^{2+} coordination. Molecular dynamics simulations of Cu^{2+} bound to the assembled OR_4 model ($Cu{:}OR_4$) reveal a close association of specific Trp and Gly residues with the Cu^{2+} center. This low Cu^{2+}-occupancy form of prion protein is redox-active and can readily initiate cleavage of the OR region, mediated by reactive oxygen species generated by Cu^{+}. The OR region is known to be required for β-cleavage, as are the Trp residues within the OR region. The β-cleaved form of the prion protein accumulates in amyloid fibrils. Hence, the close approach of Trp and Gly residues to the Cu^{2+} coordination site in the low Cu^{2+}-occupancy form of the OR region may signal an important interaction for the initiation of prion disease.

INTRODUCTION

Prion diseases, or transmissible spongiform encephalopathies, are a family of neurodegenerative diseases that occur in humans and several animals. They may arise spontaneously through inheritance, or may be acquired through alternative routes such as the ingestion of prion-contaminated foodstuffs (1). Much interest in the prion protein (PrP) has been generated from its central role in prion disease. However, to date, the physiological function(s) of the cellular form of the protein (PrP^{C}) remain unclear. The PrP^{C} was proposed to function as a copper-buffering protein (2,3), and to play a role in neuronal development (4), neuroprotection (2,4,6,7), and possibly memory (8).

The octarepeat (OR) region is located in the flexible disordered N-domain of human PrP, and consists of four tandem repeats containing the sequence PHGGGWGQ (Fig. 1). Spontaneous and inherited gene mutations that give rise to additional copies of the OR sequence in PrP were implicated as risk factors for Creutzfeldt-Jakob disease (9,10). Mice expressing an OR-deletion form of PrP demonstrated delayed prion-disease onset and altered disease pathology after exposure to infectious prion material (11). The OR region can selectively bind Cu^{2+} (12) through as many as three dissimilar coordination modes, depending on the pH and/or local Cu^{2+} concentration, corresponding to high-occupancy, intermediate-occupancy, or low-occupancy forms (13). In addition, His-96, His-111, and the N-terminal amine in the full-length N-domain can also contribute to Cu^{2+} coordination in the full-length protein (14). Under low Cu^{2+}-occupancy conditions, copper coordination to the full-length N-terminal domain results in multiple His-bound isomeric forms, primarily involving the OR region and His-96 (15). The Cu^{2+} binding to isolated fragments of the OR region was studied extensively, using spectroscopic methods (16–18). Multiple forms of copper (II) coordination occur throughout the disordered N-terminal region of the PrP at pH 7.4. However, there is limited information regarding the protein's three-dimensional (3D) structure after Cu^{2+} binding to the OR region. A small-molecule crystal structure of Cu^{2+} bound to the HGGGW residues of a single repeat was described (19), and is indicative of the binding mode of the OR region under conditions of high copper occupancy. This binding mode was recently used in extended molecular-dynamics (MD) simulations to predict how the OR region folds in response to high Cu^{2+} occupancy (7). Models were also proposed for the intermediate form of Cu^{2+} binding, based on spectroscopic data, mostly from electron paramagnetic resonance, circular dichroism, and nuclear magnetic resonance (NMR) spectroscopy (13,18). Electron paramagnetic resonance reveals that Cu^{2+} is bound by several imidazole N-donor ligands in the low-occupancy form, and its spectroscopic fingerprint is indistinguishable from that of Cu^{2+} in the presence of 50-M excess imidazole (13), indicating that the His imidazole side chains from each repeat are the primary ligands involved in coordination. Under low copper occupancy conditions, the metal center was

Submitted June 9, 2008, and accepted for publication August 21, 2008.

Address reprint requests to Hans J. Vogel, Structural Biology Research Group, Dept. of Biological Sciences, University of Calgary, Calgary, Alberta T2N 1N4, Canada. Tel.: 403-220-6006; Fax: 403-289-9311; E-mail: vogel@ucalgary.ca.

M. Jake Pushie's present address is Department of Geological Sciences, University of Saskatchewan, Saskatoon, Saskatchewan S7N 5E2, Canada.

Editor: Ruth Nussinov.

0006-3495/08/12/5084/08 $2.00

doi: 10.1529/biophysj.108.139568

humanPrP(52-94)	~PQGGGWGQ(PHGGGWGQ)$_4$GGG~
OR4 model	Ac-GGWGQ(PHGGGWGQ)$_4$-NH_2
OR2 model	Ac-PHGGGWGQPHGGGW-NH_2

FIGURE 1 Sequences of OR_4 and OR_2 peptide models, compared with a portion of human PrP sequence.

shown to be redox-active, giving rise to the formation of reactive oxygen species (ROS) and ROS-mediated cleavage of PrP^C (20–22). The cleavage site, termed β-cleavage, is around Gly-90, near the end of the OR region.

Normal proteolytic processing of membrane-anchored PrP^C occurs through cleavage at position 111/112, termed α-cleavage (18), which leaves PrP(112–231) anchored to the cell surface. However, in prion-diseased brains, longer PrP fragments accumulate in amyloid fibrils comprised of PrP(~90–231), with some variability in the site of cleavage (18). The OR region is necessary for ROS formation, and an OR-deletion form of PrP results in a loss of β-cleavage and increased sensitivity to oxidative stress (23). Loss of β-cleavage was linked to a loss of function of PrP^C (6), and may therefore be an important component in a protective mechanism for clearing oxidants in the extracellular neuronal environment. Two disease-associated PrP mutations failed to undergo β-cleavage, and $PrP^{-/-}$ cells, as well as cells expressing PrP without the OR region, are more susceptible to oxidative stress (22). Without this protective capacity, PrP is susceptible to oxidative modification (oxidative damage is also a hallmark of prion disease), and such alterations increase the protein's propensity to aggregate (24,25).

In determining how Cu^{2+}-mediated ROS formation and subsequent β-cleavage may occur, molecular modeling represents a necessary first step, because the inherent flexibility of this portion of the PrP and the paramagnetic properties of Cu^{2+} make it difficult to apply conventional structure-determination methods such as x-ray crystallography or NMR spectroscopy methods. Predicting the folded structure of a protein a priori is problematic. The backbone of each amino acid in a protein may have at least two stable conformations, and to predict how n-residues could fold together would require sampling as many as 2^n conformations. For the OR region of human PrP, this would involve a minimum of 2^{32} (~4.3 billion) conformations. The method we use here for generating a starting structure of the globular form of the metal-free OR_4 region follows an approach that resembles the zipping-and-assembly procedure of Ozkan et al. (26), where the average structure of a smaller metal-free fragment, as previously described (7), is used to assemble a starting conformation of the full-length OR region. The repetitive nature of the OR region (Fig. 1) makes it particularly amenable to such an approach.

Computational procedure

Assembly of OR_4 model

The full-length OR_4 model includes the GGWGQ portion of the non-Cu^{2+}-binding sequence that precedes the four ORs in human PrP. Previous metal-free OR_2 simulations (7) showed a preference for the formation of a well-defined bend in the GWGQ region of the OR region, whereas the PHGG portion of the sequences formed flexible loops (Fig. 2). Based on apo-OR_2 simulations, the average ϕ and ψ angles for each residue in the PHGG loop and GWGQ bend were used to construct an average structure for the full-length OR region (Fig. 2).

Cu^{2+} binding site

Each of the four His side chains in the assembled model is closely packed and already suitably clustered together to accommodate coordination of a metal ion. The His χ_1 and χ_2 angles were modified to produce suitable starting structures for Cu^{2+} coordination, where either all Nδ1-atoms or Nε2-atoms were oriented toward a common center for insertion of a Cu^{2+} atom. In the copper-free OR_2 simulations, close association between His side chains was also evident, as shown in Fig. S7 in Supplementary Material, Data S1.

Density functional theory modeling and derivation of $\Delta G^{calc}_{(aq)}$

Small-molecule structure models of the His side chain were modeled as 4-methylimidazole, in two alternate protonation

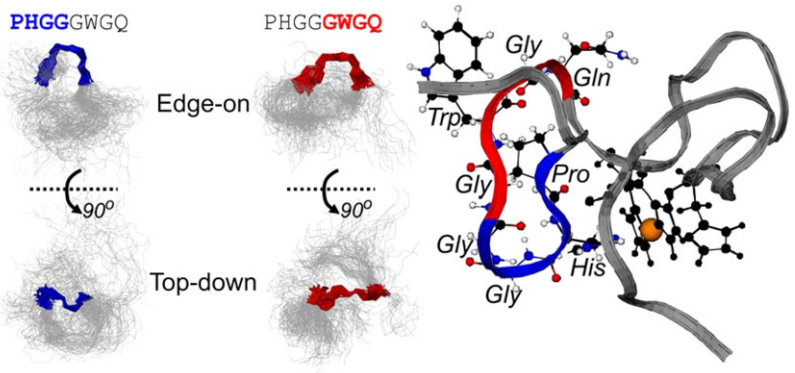

FIGURE 2 Stable structures of PHGG and GWGQ portions of a single octarepeat (OR) were derived from two 130-ns metal-free OR_2 MD simulations and used to assemble the Cu:OR_4 model. RMS-fitted overlays of PHGG and GWGQ portions of the OR_2 model are shown in two orientations. Loops and turns of the PHGG and GWGQ regions are emphasized. The PHGG and GWGQ residues in a representative OR of the assembled Cu:OR_4 model are highlighted. The remaining His residues and the copper center in the Cu:OR_4 model are shown for clarity.

states or Cu^{2+}-bound states (Fig. 3). The Cu^{2+} complexes were modeled as $[Cu^{II}(4\text{-methylimidazole})(OH_2)_3]^{2+}$. All density functional calculations were performed with the Gaussian 03 suite of software (27). Geometry optimizations were performed at the B3LYP/6-31G(d) level, until the difference in energy between subsequent optimization steps was below 0.03 kJ mol^{-1}. This step also included harmonic-frequency calculations, from which zero-point vibrational energies, temperature-dependent enthalpy corrections, and entropies were derived. Single-point energy calculations from B3LYP/6-31G(d) structures were computed, using a larger basis set to obtain more accurate relative energies between structures (B3LYP/6-311+G(2df,2p)). Solvation was taken into account using a polarizable continuum model, IEFPCM (28–30), with the radius for Cu^{2+} as 1.40 Å, and the dielectric constant set at 78.39 (water).

The aqueous free-energy change ($\Delta G^{calc}_{(aq)}$) is calculated as:

$$\Delta G^{calc}_{(aq)} = \Delta H_{(g)} - T\Delta S_{(g)} + \Delta\Delta G_{(solv)},$$

where $\Delta H_{(g)}$ and $\Delta S_{(g)}$ are the energy and entropy difference between product and reactant enthalpies, $\Delta H_{(g)}$ is corrected to 298 K and includes the zero-point energy, and $\Delta S_{(g)}$ is the entropy difference between species, as provided in the frequency-calculation output. The $\Delta\Delta G_{(solv)}$ term is the difference between the free energy of solvation ($\Delta G_{(solv)}$) for the product and reactant species.

Initial Cu^{2+}-bound OR_4 geometry setup

Short-duration simulations were run with a single Cu^{2+}-atom bound through either the Nδ1-atoms or Nε2-atoms of all four His residues. These initial models contained Cu^{2+} close to the desired His N-donor atoms, and were energy-minimized by steepest descent in the absence of solvent molecules, using GROMACS (31,32) and the OPLS all-atom force field (33,34). After energy minimization, the Cu_1:OR_4 models were simulated for 100 ps to relax the Cu^{2+}-binding region.

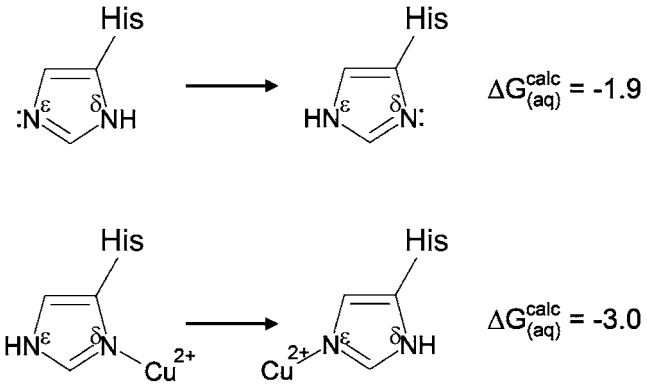

FIGURE 3 Tautomeric forms of His side chain, modeled as 4-methylimidazole. Theory and experiment both predict the Nε2-position as the favored site for protonation. Alternate sites of Cu^{2+} coordination are compared, and modeled as $[Cu^{II}(4\text{-methylimidazole})(OH_2)_3]^{2+}$ (coordinating solvent not depicted). Relative free energies are in kJ mol^{-1}.

This procedure generated structures that could be subsequently simulated in the presence of solvent.

MD simulation

After the generation of the starting geometries, each molecule was placed in a 4.5 × 4.5 × 4.5 nm box, surrounded by 2836 SPC solvent molecules (35,36). Two Cl^- counterions were also added, to maintain the charge neutrality of the copper-containing system. Each of the systems was energy-minimized in the presence of explicit solvent, and simulated for 200 ns at 300 K, with an initial 5-ns equilibration phase. Simulations were subsequently performed according to previously described methods (7).

Parameterization of Cu^{2+} binding models

Alternate Nδ1-bound and Nε2-bound $[Cu^{II}(4\text{-methylimidazole})_4]^{2+}$ models were geometry optimized at the B3LYP/6-31G(d) level, until the difference in energy between subsequent optimization steps was below 0.03 kJ mol^{-1}. The geometry-optimization step was followed by a harmonic-frequency calculation at the same level of theory, to ensure that geometries were at a stationary point on the potential energy surface, and to derive force constants for Cu-ligand bonds.

The CHelpG charges (37) were calculated for each of the structures at the B3LYP/6-31G(d) level. Calculated parameters were imported into the OPLS all-atom force field, following previously described methods (7). The CHelpG charges for the copper centers in each of the $[Cu^{II}(4\text{-methylimidazole})_4]^{2+}$ models were averaged to +0.700. The backbone charges for His residues were maintained from the OPLS force field, whereas the imidazole ring and $C\beta H_2$ fragments had a net charge of +0.325 each, making the total charge for the copper$(His)_4$ binding sites +2.000. In the Nδ1-bound Cu:OR_4 simulations, the Cu^{2+}-N-donor atom distances were all 1.985 Å, averaged from the associated Nδ1-bound $[Cu^{II}(4\text{-methylimidazole})_4]^{2+}$ models, and the force constants for each of the Cu-N bonds were 45,082 kJ mol^{-1} nm^{-2}. The Nε2-bound Cu:OR_4 simulations used a Cu^{2+}-N-donor atom distance of 1.914 Å, with force constants of 46,346 kJ mol^{-1} nm^{-2}. The Cu^{2+} centers were in a pseudosquare planar geometry, based on the coordination geometries of the calculated $[Cu^{II}(4\text{-methylimidazole})_4]^{2+}$ models, and were of pseudo-D_{2d} symmetry. The parameters for restraining the coordination geometries in MD simulations used improper dihedral force constants of 33.472 kJ mol^{-1} rad^{-2}.

RESULTS

Generation of starting conformation of OR_4 model

Using the results of previously described MD simulations (7) as well as additional simulations containing modified force-

field parameters for tryptophan, a total of 300 ns of simulation time was generated for the copper-free OR_2 model (Fig. 1). Cluster analysis was used to group each of the visited conformations with similar conformations from all simulations, based on a root mean-square deviation (RMSD) cutoff of 0.1 nm, and included all residues in the OR_2 model. The PHGG and GWGQ residues from the major cluster of each simulation, corresponding to the most populated conformation shown in Fig. 2, were then used to generate average ϕ and ψ angles for each residue.

The mean ϕ and ψ angles were input for each series of PHGG and GWGQ residues in the OR_4 model. The assembled structure (Fig. 2) contains no other overlapping atoms or side-chain clashes, aside from initially overlapping His imidazole rings (not shown). The His side chains in the OR_2 models were also seen to make prolonged close approaches to one another (Fig. S7 in Data S1). The close packing of His side chains in the assembled model present a preformed site suitable for coordination of a single Cu^{2+} atom. The His side-chain χ_1 and χ_2 angles were subsequently modified, so that either the Nδ1-atoms or Nε2-atoms were suitably oriented to coordinate a central Cu^{2+} atom, as depicted in Fig. 2.

Histidine side-chain tautomers and Cu^{2+} coordination sites

The His side chain contains two N-atoms that confer the imidazole ring with multiple protonation states, and at physiological pH, two tautomeric forms of the charge-neutral imidazole ring may exist, as shown in Fig. 3. These tautomeric forms differ in the site of protonatation, at either the Nδ1-atom or Nε2-atom. Experimentally, a slight preference was found for protonation at the Nε2 position of the imidazole ring at physiological pH, meaning that the Nδ1-atom is most likely to bear the lone electron pair (38–40). The calculated aqueous free-energy difference ($\Delta G^{\mathrm{calc}}_{(\mathrm{aq})}$) for the two tautomeric forms of His, modeled as 4-methylimidazole, is -1.9 kJ mol^{-1}, slightly favoring protonation at the Nε2-atom position. This agrees with the experimentally observed equilibrium for His (38,39). The real $\Delta G_{(\mathrm{aq})}$ for the amino acid has further contributions from H-bonds that stabilize this tautomer through the Nδ1-atom lone pair and adjacent backbone amide protons (39,41).

The $\Delta G^{\mathrm{calc}}_{(\mathrm{aq})}$ between the two tautomeric forms for the site of copper coordination, at either the Nδ1-atom or Nε2-atom position, modeled as $[Cu^{II}(4\text{-methylimidazole})(OH_2)_3]^{2+}$, reveals that the N$\varepsilon$2-bound form is 3.0 kJ mol^{-1} more stable than the Nδ1-bound form (Fig. 3). This indicates that coordination through the ε N-atom is likely. Miura et al. observed that at pH ~6.5, the OR_4 region binds Cu^{2+} via the Nε2-atoms, whereas at lower pH, the His side chains protonate, making them unavailable for coordination, and as pH is increased, coordination via the Nδ1-atoms is ultimately preferred (42). Thus, coordination of Cu^{2+} via the Nε2-atom site appears to be preferred. However, the small free-energy difference for Cu^{2+} coordination, as shown in Fig. 3, led us to model two alternate coordination modes for the Cu^{2+}:OR_4 model, with His coordination through either four Nδ1-atoms or four Nε2-atoms concurrently.

Average Cu^{2+}:OR_4 structures

No stable helical or β-sheet structures formed during MD simulations of the assembled structures, in agreement with the lack of secondary structure evidenced by circular dichroism spectroscopy (43,44). Comparing results from the Nδ1-bound and Nε2-bound Cu^{2+}:OR_4 models, coordination by all four Nδ1-atoms of the His residues maintains a more compact globular form of the OR_4 region, whereas Nε2-coordination tends to fan each OR loop outward (Fig. 4) during a simulation. The Nδ1-bound form also sequesters the metal center more than does the Nε2-bound form, which maintains a solvent-exposed metal-binding site (Fig. 4). The RMS-fitted overlays from the final 20 ns of the $(PHGGGWGQ)_3PH$ portions of each Cu^{2+}:OR_4 model, as well as each individual repeat (numbered OR1 through OR4) from each simulation, are shown in Fig. 4. Once anchored to the Cu^{2+} center through the His side chains, each repeat deviates little from its initial average conformation. The N-terminal and C-terminal ends of the model comprise the preceding GGWGQ, and the terminating GWGQ residues are disordered and display greater flexibility than the remaining OR_4 regions in the course of simulations. Additional RMSD data are presented in Fig. S8 in Data S1.

Tryptophan and glycine residues in the OR region can interact with bound Cu^{2+}

The peptide backbone of much of the Nδ1-bound and Nε2-bound models is held away from the metal center because of coordination via the His imidazole side chains. This makes interactions between other portions of the OR region with the metal coordination site less likely. In the Nδ1-bound Cu:OR_4 system (Fig. 4), although the metal center is somewhat sequestered from access by solvent, a portion of the fourth repeat can come into close contact with the Cu^{2+} ion, whereas in the Nε2-bound form, a portion of the fourth repeat as well as the third repeat can both make transient close approaches to the metal coordination site.

The Trp residues, located at the turns in the OR loops between the successive Cu^{2+}-binding His residues, are always solvent-exposed during simulations. On average, the Trp-Cu^{2+} internuclear separation (measured between the Trp indole Nε1-atom and Cu^{2+}) for all Trp residues in both the Nε2-bound and Nδ1-bound simulations is 10 Å or greater. Specific Trp residues in each simulation, however, demonstrate significantly closer approaches to the metal center, such as the Trp residue from the third repeat in the Nε2-bound model and the Trp residue from the fourth repeat in the Nδ1-bound model. In these instances, the Trp-Cu^{2+} separation

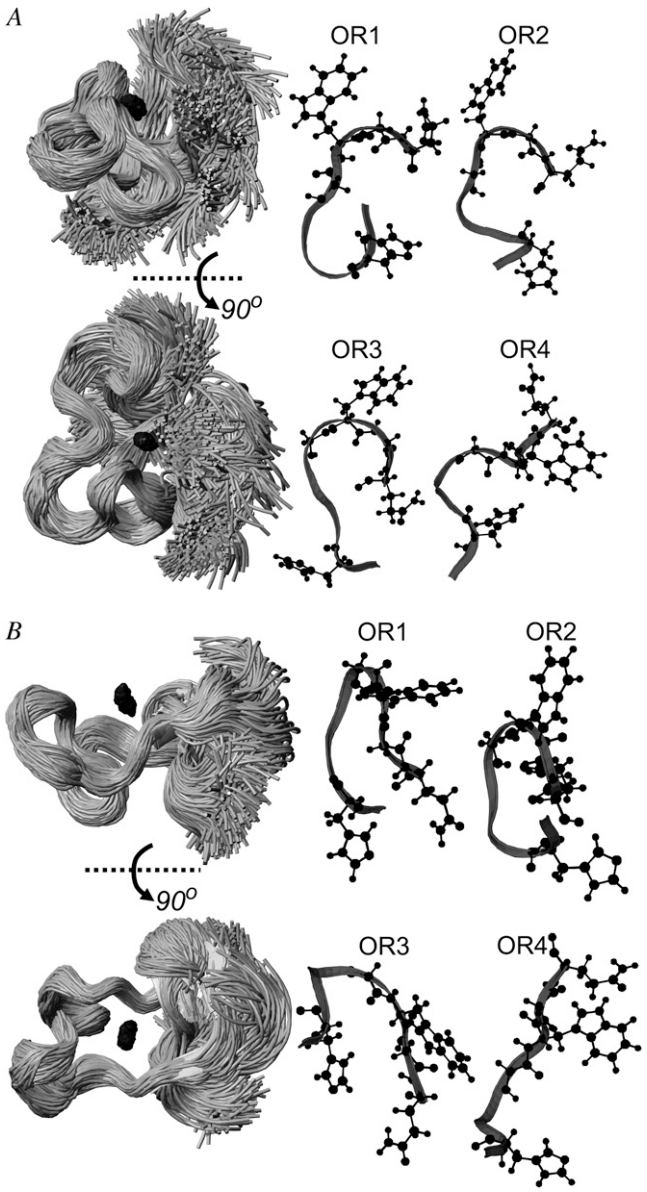

FIGURE 4 The Nδ1- and Nε2-bound complexes (*A* and *B*, respectively) were each simulated for 200 ns. Overlays of 2000 structures from the final 20 ns of each simulation, shown in two orientations, are RMS-fitted, using $(PHGGGWGQ)_3PH$ backbone heavy atoms. The major conformation of each octarepeat is shown, with Cu^{2+}-binding His and GWGQ residues explicitly drawn. Numbering from the human PrP sequence is shown.

may be as low as 6–7 Å (Fig. 5 *A*). A summary of all Trp Nε1-Cu^{2+} internuclear separations from each simulation are presented in Fig. S9 in Data S1.

Applicability of Cu:OR_4 models

The procedure of constructing copper-binding OR_4 models through assembly has some specific assumptions associated with it. Firstly, the assembled OR_4 structure assumes that all four OR regions will cooperatively fold in the same manner as they do in the copper-free OR_2 models from which they are derived. Secondly, coordination by all four His residues concurrently does not allow for additional conformational flexibility within the OR region. Each of these points is addressed below.

Previous NMR experiments by Yoshida et al. (45) and Zahn (46) revealed that the OR region adopts loop and turn-type structures, which are also formed in our apo-OR_2 models (7). These experimental observations lend indirect support to the conformation of the preformed copper-coordinating structure that we established through the assembly of OR fragments.

The ability of His ligands to become labile and exit the coordination sphere would not only allow those regions of the backbone greater flexibility, but could also allow for further variability in Cu^{2+}-coordination when the His imidazole reenters the coordination sphere, with the possibility that an alternate imidazole N-donor atom may coordinate to copper, or alternate backbone conformations may be accessible. This type of exchange in the ligand environment could in principle give rise to 16 alternate four-coordinate geometries (4^2), and as many local potential energy surfaces to explore. Further consideration of intermediate coordination geometries, e.g., by only three His residues, could further increase the complexity and number of possible models.

Taking these considerations into account, the models presented here comprise the most tractable initial approach to understanding the low-Cu^{2+}-occupancy form of the OR region. The Cu^{2+} coordination via Nε2-atoms of the His residues in the Cu_1OR_4 model is in agreement with the previously observed coordination mode of the OR_4 peptide at pH 6.5 by Raman spectroscopy (42).

DISCUSSION

The Trp residues within the OR region were shown to be necessary for the redox competence of the low-occupancy form of Cu^{2+} bound to the OR region of PrP (47), whereas successive binding of Cu^{2+} renders the metal ions redox-inactive. The consequence of Cu^{2+} binding in the low-occupancy, redox-active form is ROS formation and subsequent β-cleavage of the OR region from the remainder of membrane-anchored PrP^C. The Trp residues may act as one-electron donors, facilitating reduction of the single Cu^{2+} center to Cu^+, within the OR region. Our MD simulations implicate a close association between the bound Cu^{2+} atom and specific Trp residues within the OR region.

The only Trp residues from either series of simulations to make a significantly close approach to the Cu^{2+} ion are Trp-80 and Trp-89. However, other Trp residues may occasionally come to within 10 Å as well. A previous model from Miura et al. indicated that Trp-65 and Trp-73 could interact with Cu^{2+} (42). Because their model was derived by only constraining the coordinating His residues to remain bound to the Cu^{2+} center, without accounting for the folding preference

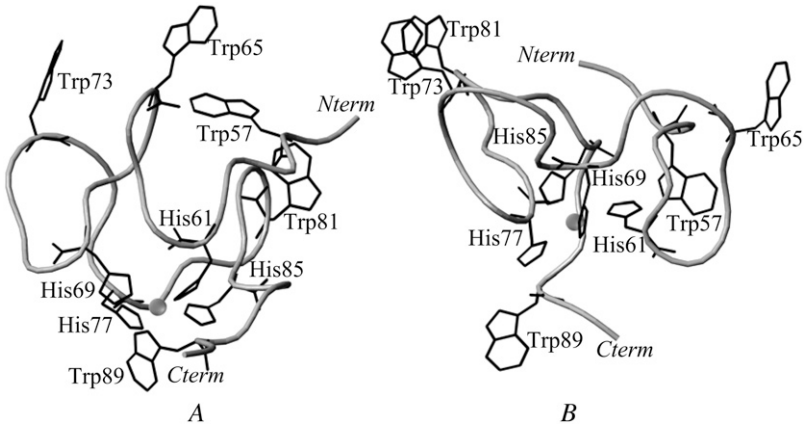

FIGURE 5 Snapshots of the close approach of Trp residues to the Cu^{2+}-binding site in (*A*) Nε2-bound and (*B*) Nδ1-bound models from MD simulations. Each of the His and Trp side chains is drawn for clarity. Nterm and Cterm denote the N-terminal and C-terminal ends of the sequence, respectively.

of the sequence, we are inclined to assert that Trp-80 and Trp-89 (from the two C-terminal repeats) are important for β-cleavage. These observations beg the question of whether such interactions may play a role in the ability of the OR region to reduce Cu^{2+} to Cu^{+} during ROS formation. In addition to Cu^{2+} coordination, the four-His coordination environment of the OR region is also compatible with Cu^{+} binding. The OR_4 region is sufficiently flexible to accommodate the tetrahedral coordination geometry required for stabilizing Cu^{+} formation.

As noted earlier, the assembled OR_4 models can accommodate tetrahedral coordination geometry, and are not only compatible with Cu^{+} binding, but with Zn^{2+} coordination as well (data not shown). Copper and zinc binding to the N-terminal domain triggers endocytosis of PrP (48), and these models offer further structural details that may be used to refine structure interactions with neighboring regions of PrP and micelle environments (49), as well as offer insights into the initial events leading to β-cleavage. The structures presented here may provide the first clues that relate Cu^{2+} binding, ROS formation, and the site specificity of β-cleavage.

Because β-cleavage is the result of ROS formation, it is likely that the site at which reactive species are formed is at, or near, the site of cleavage. Generation of ROS at a more remote site would require the formation of diffusible ROS that would ultimately result in less site-specific cleavage, indicating that the site of ROS formation likely involves the initial close approach of the protein backbone to the metal center. Several repeats in each of the series of simulations make such an approach to the metal center, and both the Cα-atoms of Trp (residue 89) and Gly (residue 90) make transient approaches to within <6 Å of the Cu^{2+} center in the Nδ1-bound simulation, as shown in Fig. 5 *B*. Similar interaction with other repeats in alternate conformations may provide a structural mechanism for ROS-mediated β-cleavage within the OR region.

Our proposed mechanism for copper-mediated ROS formation, shown in Fig. 6, is initiated by close association of Trp with the Cu^{2+} center, followed by subsequent electron transfer from the Trp indole to form Cu^{+}. In the presence of H_2O_2, Cu^{+} is readily oxidized back to Cu^{2+}, and results in the formation of HO^{-} and $HO^{\cdot}$. Hydroxyl radicals are highly reactive, and are likely to react at or near their site of formation: in this instance, through H-atom abstraction from a nearby aliphatic group. Because of the high abundance of Gly residues in the OR region (Fig. 1), the local protein backbone contains multiple potential targets for H-atom abstraction. Hydroxyl radical damage at a Gly residue results in a C-centered radical, and the subsequent reaction of Gly(C$\alpha^{\cdot}$) with O_2 triggers C-N or C-C backbone cleavage within the

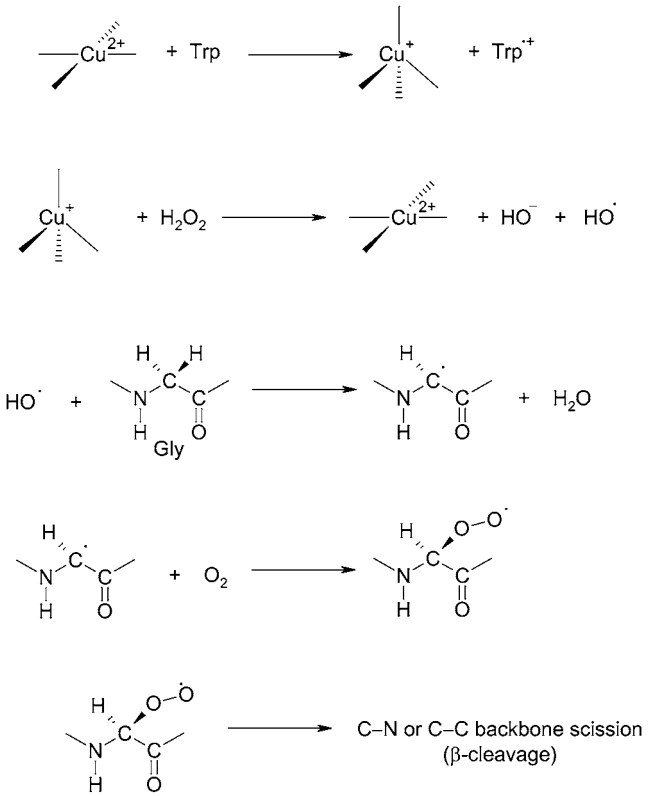

FIGURE 6 Mechanism of copper-mediated hydroxyl radical formation and subsequent β-cleavage of protein backbone. Copper coordination environments for Cu^{2+} and Cu^{+} are depicted as their preferred square planar and tetrahedral geometry respectively, both of which can be accommodated by the flexible octarepeat region of PrP.

damaged residue. The most likely Gly residues to be targets of $HO^{\cdot}$ attack would be those closest to the Cu^{2+} center. The close approach of Trp-89 and each of its adjacent Gly residues, as observed in these simulations, lends support for their proximity to this potential ROS-generating site. The formed Trp indole radical cation ($Trp^{\cdot+}$) may undergo subsequent reactions, including deprotonation at the indole N(H) site, as well as cross-linking reactions with other $Trp^{\cdot+}$ residues. It may also be possible that $Trp^{\cdot+}$ plays a role in directing β-cleavage of the local protein backbone. However, further work would be necessary to establish a mechanistic link.

Previous experiments (50) suggested that copper-binding to PrP can induce a proteinase-resistant form of PrP, possibly through folding in the N-domain. Although it is clear that the OR region can become structured in response to increasing copper loads, recent evidence indicates that copper itself inhibits proteinase-K, and therefore cannot be used to infer the presence of specific structuring within PrP in this manner (51).

These structures provide the first account of the conformation of the OR region under conditions of low-Cu^{2+}-occupancy in mammalian PrP. The OR region was recently shown to bind Zn^{2+} in a manner similar to that of Cu^{2+} (52), and these structures are also compatible with Zn^{2+} coordination. These results are a necessary first step toward more elaborate structural models for Cu^{2+}-binding to this region of PrP, and toward understanding the associated redox activity of PrP-bound copper and their relationship to prion disease.

SUPPLEMENTARY MATERIAL

To view all of the supplemental files associated with this article, visit www.biophysj.org.

The authors are indebted to Dr. Arvi Rauk and Dr. Frank Jirik for numerous stimulating discussions regarding the topic of this study.

M.J.P. is supported by an Alberta Ingenuity Studentship, and H.J.V. holds a Scientist Award from the Alberta Heritage Foundation for Medical Research. This research was enabled by the use of WestGrid computing resources, which are funded in part by the Canada Foundation for Innovation, Alberta Innovation and Science, British Columbia Advanced Education, and participating research institutions.

REFERENCES

1. Prusiner, S. B. 1982. Novel proteinaceous infectious particles cause scrapie. *Science*. 216:136–144.
2. Vassallo, N., and J. Herms. 2003. Cellular prion protein function in copper homeostasis and redox signalling at the synapse. *J. Neurochem.* 86:538–544.
3. Westergard, L., H. M. Christensen, and D. A. Harris. 2007. The cellular prion protein (PrP^{C}): its physiological function and role in disease. *Biochim. Biophys. Acta*. 1772:629–644.
4. Salěs, N., R. Hassig, K. Rodolfo, L. Di Giamberardino, E. Traiffort, M. Ruat, P. Fretier, and K. L. Moya. 2002. Developmental expression of the cellular prion protein in elongating axons. *Eur. J. Neurosci.* 15:1163–1177.
5. Reference deleted in proof.
6. Mitteregger, G., M. Vosko, B. Krebs, W. Xiang, V. Kohlmannsperger, S. Nolting, G. F. Hamann, and H. A. Kretzschmar. 2007. The role of the octarepeat region in neuroprotective function of the cellular prion protein. *Brain Pathol.* 17:174–183.
7. Pushie, M. J., and H. J. Vogel. 2007. Molecular dynamics simulations of two tandem octarepeats from the mammalian prion protein: fully-Cu^{2+}-bound and metal-free forms. *Biophys. J.* 93:3762–3774.
8. Tompa, P., and P. Friedrich. 1998. Prion proteins as memory molecules: an hypothesis. *Neuroscience*. 86:1037–1043.
9. Collinge, J., A. E. Harding, F. Owen, M. Poulter, R. Lofthouse, A. M. Boughey, T. Shah, and T. J. Crow. 1989. Diagnosis of Gerstmann-Sträussler syndrome in familial dementia with prion protein gene analysis. *Lancet*. ii:15–17.
10. Owen, F., M. Poulter, R. Lofthouse, J. Collinge, T. J. Crow, D. Risby, H. F. Baker, R. M. Ridley, K. Hsiao, and S. B. Prusiner. 1989. Insertion in prion protein gene in familial Creutzfeldt-Jakob disease. *Lancet*. i:51–52.
11. Flechsig, E., D. Shmerling, I. Hegyi, A. J. Raeber, M. Fischer, A. Cozzio, C. von Mering, A. Aguzzi, and C. Weissmann. 2000. Prion protein devoid of the octapeptide repeat region restores susceptibility to scrapie in PrP knockout mice. *Neuron*. 27:399–408.
12. Stöckel, J., J. Safar, A. C. Wallace, F. E. Cohen, and S. B. Prusiner. 1998. Prion protein selectively binds copper(II) ions. *Biochemistry*. 37:7185–7193.
13. Chattopadhyay, M., E. D. Walter, D. J. Newell, P. J. Jackson, E. Aronoff-Spencer, J. Peisach, G. J. Gerfen, B. Bennett, W. E. Antholine, and G. L. Millhauser. 2005. The octarepeat domain of the prion protein binds Cu(II) with three distinct coordination modes at pH 7.4. *J. Am. Chem. Soc.* 127:12647–12656.
14. Klewpatinond, M., P. Davies, S. Bowen, D. R. Brown, and J. H. Viles. 2008. Deconvoluting the copper^{2+} binding modes of full-length prion protein. *J. Biol. Chem.* 283:1870–1881.
15. Srikanth, R., J. Wilson, C. S. Burns, and R. W. Vachet. 2008. Identification of the copper(II) coordinating residues in the prion protein by metal-catalyzed oxidation mass spectrometry: evidence for multiple isomers at low copper(II) loadings. *Biochemistry*. In press.
16. Pushie, M. J., and H. J. Vogel. 2007. Mass spectrometric determination of the coordination geometry of potential copper(II) surrogates for the mammalian prion protein octarepeat region. *Anal. Chem.* 79:5659–5667.
17. Weiss, A., P. Del Pino, U. Bertsch, C. Renner, M. Mentler, K. Grantner, L. Moroder, H. A. Kretzschmar, and F. G. Parak. 2007. The configuration of the Cu^{2+} binding region in full-length human prion protein compared with the isolated octapeptide. *Vet. Microbiol.* 123:358–366.
18. Wells, M. A., C. Jelinska, L. L. Hosszu, C. J. Craven, A. R. Clarke, J. Collinge, J. P. Waltho, and G. S. Jackson. 2006. Multiple forms of copper (II) co-ordination occur throughout the disordered N-terminal region of the prion protein at pH 7.4. *Biochem. J.* 400:501–510.
19. Burns, C. S., E. Aronoff-Spencer, G. Legname, S. B. Prusiner, W. E. Antholine, G. J. Gerfen, J. Peisach, and G. L. Millhauser. 2003. Copper coordination in the full-length, recombinant prion protein. *Biochemistry*. 42:6794–6803.
20. Mangé, A., F. Béranger, K. Peoc'h, T. Onodera, Y. Frobert, and S. Lehmann. 2004. α- and β-cleavages of the amino-terminus of the cellular prion protein. *Biol. Cell*. 96:125–132.
21. McMahon, H. E., A. Mange, N. Nishida, C. Creminon, D. Casanova, and S. Lehmann. 2001. Cleavage of the amino terminus of the prion protein by reactive oxygen species. *J. Biol. Chem.* 276:2286–2291.
22. Watt, N. T., and N. M. Hooper. 2005. Reactive oxygen species (ROS)-mediated β-cleavage of the prion protein in the mechanism of the cellular response to oxidative stress. *Biochem. Soc. Trans.* 33:1123–1125.
23. Watt, N. T., D. R. Taylor, A. Gillott, D. A. Thomas, W. S. Perera, and N. M. Hooper. 2005. Reactive oxygen species-mediated β-cleavage of the prion protein in the cellular response to oxidative stress. *J. Biol. Chem.* 280:35914–35921.
24. Requena, J. R., D. Groth, G. Legname, E. R. Stadtman, S. B. Prusiner, and R. L. Levine. 2001. Copper-catalyzed oxidation of the recombinant

SHa(29–231) prion protein. *Proc. Natl. Acad. Sci. USA*. 98:7170–7175.

25. Robert, B., R. B. Petersen, S. L. Siedlak, H. Lee, Y. Kim, A. Nunomura, F. Tagliavini, B. Ghetti, P. Cras, P. I. Moreira, R. J. Castellani, M. Guentchev, H. Budka, J. W. Ironside, P. Gambetti, M. A. Smith, and G. Perry. 2005. Redox metals and oxidative abnormalities in human prion diseases. *Acta Neuropathol. (Berl.)*. 110:232–238.
26. Ozkan, B. S., G. A. Wu, J. D. Chodera, and K. A. Dill. 2007. Protein folding by zipping and assembly. *Proc. Natl. Acad. Sci. USA*. 104: 11987–11992.
27. Frisch, M. J., G. W. Trucks, H. B. Schlegel, G. E. Scuseria, M. A. Robb, J. R. Cheeseman, J. A. Montgomery, Jr., T. Vreven, K. N. Kudin, J. C. Burant, J. M. Millam, S. S. Iyengar, J. Tomasi, V. Barone, B. Mennucci, M. Cossi, G. Scalmani, N. Rega, G. A. Petersson, H. Nakatsuji, M. Hada, M. Ehara, K. Toyota, R. Fukuda, J. Hasegawa, M. Ishida, T. Nakajima, Y. Honda, O. Kitao, H. Nakai, M. Klene, X. Li, J. E. Knox, H. P. Hratchian, J. B. Cross, V. Bakken, C. Adamo, J. Jaramillo, R. Gomperts, R. E. Stratmann, O. Yazyev, A. J. Austin, R. Cammi, C. Pomelli, J. W. Ochterski, P. Y. Ayala, K. Morokuma, G. A. Voth, P. Salvador, J. J. Dannenberg, V. G. Zakrzewski, S. Dapprich, A. D. Daniels, M. C. Strain, O. Farkas, D. K. Malick, A. D. Rabuck, K. Raghavachari, J. B. Foresman, J. V. Ortiz, Q. Cui, A. G. Baboul, S. Clifford, J. Cioslowski, B. B. Stefanov, G. Liu, A. Liashenko, P. Piskorz, I. Komaromi, R. L. Martin, D. J. Fox, T. Keith, M. A. Al-Laham, C. Y. Peng, A. Nanayakkara, M. Challacombe, P. M. W. Gill, B. Johnson, W. Chen, M. W. Wong, C. Gonzalez, and J. A. Pople. 2004. Gaussian 03, Revision C.02. Gaussian, Wallingford, CT.
28. Cancès, M. T., B. Mennucci, and J. Tomasi. 1997. A new integral equation formalism for the polarizable continuum model: theoretical background and applications to isotropic and anisotropic dielectrics. *J. Chem. Phys.* 107:3032–3041.
29. Mennucci, B., E. Cancès, and J. Tomasi. 1997. Evaluation of solvent effects in isotropic and anisotropic dielectrics, and in ionic solutions with a unified integral equation method: theoretical bases, computational implementation and numerical applications. *J. Phys. Chem. B*. 101:10506–10517.
30. Tomasi, J., B. Mennucci, and E. Cancès. 1999. The IEF version of the PCM solvation method: an overview of a new method addressed to study molecular solutes at the QM ab initio level. *J. Mol. Struct. THEOCHEM*. 464:211–226.
31. Berendsen, H. J. C., D. van der Spoel, and R. van Drunen. 1995. GROMACS: a message-passing parallel molecular dynamics implementation. *Comput. Phys. Commun*. 91:43–56.
32. Lindahl, E., B. Hess, and D. van der Spoel. 2001. GROMACS 3.0: a package for molecular simulation and trajectory analysis. *J. Mol. Model*. 7:306–317.
33. Kaminski, G., E. M. Duffy, T. Matsui, and W. L. Jorgensen. 1994. Free energies of hydration and pure liquid properties of hydrocarbons from the OPLS all-atom model. *J. Phys. Chem*. 98:13077–13082.
34. Jorgensen, W. L., D. S. Maxwell, and J. Tirado-Rives. 1996. Development and testing of the OPLS all-atom force field on conformational energetics and properties of organic liquids. *J. Am. Chem. Soc*. 118:11225–11236.
35. Berendsen, H. C., J. P. M. Postma, W. F. van Gunsteren, and J. Hermans. 1981. Interaction models for water in relation to protein hydration. *In* Intermolecular Forces. B. Pullman, editor. Reidel, Dordrecht. 331–342.
36. Berendsen, H. J. C., J. P. M. Postma, A. DiNola, and J. R. Haak. 1984. Molecular dynamics with coupling to an external bath. *J. Chem. Phys.* 81:3684–3690.
37. Carlson, H. A., T. B. Nguyen, M. Orozco, and W. L. Jorgensen. 1993. Accuracy of free energies of hydration for organic molecules from 6–31G*-derived partial charges. *J. Comput. Chem*. 10:1240–1249.
38. Reynolds, W. F., I. R. Peat, M. H. Freedman, and I. R. Lyerla. 1973. Determination of the tautomeric form of the imidaozle ring of L-histidine in basic solution by carbon-13 magnetic resonance spectroscopy. *J. Am. Chem. Soc*. 95:328–331.
39. Blomberg, F., W. Maurer, and H. Rüterjans. 1977. Nuclear magnetic resonance investigation of ^{15}N-labeled histidine in aqueous solution. *J. Am. Chem. Soc*. 99:8149–8159.
40. Walters, D. E., and A. Allerhand. 1980. Tautomeric states of the histidine residues of bovine pancreatic ribonuclease A. *J. Biol. Chem.* 255:6200–6204.
41. Berlin, P., M. Kreisler, S. F. Arkhipova, G. M. Lipkind, and E. M. Popov. 1977. An investigation of the conformational states of the methylamide of N-acetyl-L-histidine. *Chem. Nat. Compd*. 12:323–328.
42. Miura, T., S. Sasaki, A. Toyama, and H. Takeuchi. 2005. Copper reduction by the octapeptide repeat region of the prion protein: pH dependence and implications in cellular copper uptake. *Biochemistry*. 44:8712–8720.
43. Wells, M. A., G. S. Jackson, S. Jones, L. L. Hosszu, C. J. Craven, A. R. Clarke, J. Collinge, and J. P. Waltho. 2006. A reassessment of copper(II) binding in the full-length prion protein. *Biochem. J*. 399:435–444.
44. Garnett, A. P., and J. H. Viles. 2003. Copper binding to the octarepeats of the prion protein. Affinity, specificity, folding and cooperativity: Insights from circular dichroism. *J. Biol. Chem*. 278:6795–6802.
45. Yoshida, H., N. Matsushima, Y. Kumaki, M. Nakata, and K. Hikichi. 2000. NMR studies of model peptides of PHGGGWGQ repeats within the N-terminus of prion proteins: a loop conformation with histidine and tryptophan in close proximity. *J. Biochem. (Tokyo)*. 128:271–281.
46. Zahn, R. 2003. The octapeptide repeats in mammalian prion protein constitute a pH-dependent folding and aggregation site. *J. Mol. Biol*. 334:477–488.
47. Ruiz, F. H., E. Silva, and N. C. Inestrosa. 2000. The N-terminal tandem repeat region of human prion protein reduces copper: role of tryptophan residues. *Biochem. Biophys. Res. Commun*. 269:491–495.
48. Pulay, P. C., and D. A. Harris. 1998. Copper stimulates endocytosis of the prion protein. *J. Biol. Chem*. 273:33107–33110.
49. Dong, S. L., S. A. Cadamuro, F. Fiorino, U. Bertsch, L. Moroder, and C. Renner. 2007. Copper binding and conformation of the N-terminal octarepeats of the prion protein in the presence of DPC micelles as membrane mimetic. *Bioploymers*. 88:840–847.
50. Qin, K., D. Yang, Y. Yang, M. A. Chishti, L. Meng, H. A. Kretzschmar, C. M. Yip, P. E. Fraser, and D. Westaway. 2000. Copper(II)-induced conformational changes and protease resistance in recombinant and cellular PrP. Effect of protein age and deamidation. *J. Biol. Chem.* 275:19121–19131.
51. Stone, L. A., G. S. Jackson, J. Collinge, J. D. F. Wadsworth, and A. R. Clarke. 2007. Inhibition of proteinase K activity by copper(II) ions. *Biochemistry*. 46:245–252.
52. Walter, E. D., D. J. Stevens, M. P. Visconte, and G. L. Millhauser. 2007. The prion protein is a combined zinc and copper binding protein: Zn^{2+} alters the distribution of Cu^{2+} coordination modes. *J. Am. Chem. Soc*. 129:15440–15441.